2011 IEEE/ASME International Conference on
Advanced Intelligent Mechatronics (AIM2011)
Budapest, Hungary, July 3-7, 2011

A Comparative Study on Active SLAM and Autonomous Exploration with Particle Filters

Jingjing Du, Luca Carlone, Miguel Kaouk Ng, Basilio Bona, and Marina Indri

Abstract— **Planning under uncertainty in perception and action requires the robot to be able to use active strategies for trading-off between the contrasting tasks of exploring the scenario and satisfying given constraints on the admissible uncertainty in the estimation process. In this work we compare several state-of-the-art approaches to *active SLAM (Simultaneous Localization and Mapping)* and exploration using Rao-Blackwellized Particle Filters. The proposed numerical evaluation and analytical insight allow to have a clear picture of the advantages and limitations of each technique for real world applications. Extensive tests are performed in typical indoor and office environments and on well-known benchmarking scenarios belonging to SLAM literature, with the purpose of evaluating the maturity of the field and the potential of truly autonomous navigation systems based on particle filtering.**

I. Introduction

In the last decades, the increasing use of mobile robotic systems in service and domestic applications has highlighted the importance of autonomous navigation. In particular, *autonomous exploration* capability is a crucial prerequisite for mission accomplishment. When no absolute localization service is available to the robot (e.g., GPS), the exploration task, which can be considered a decisional process, needs to be accompanied by the concurrent estimation of robot pose and a map of the environment. This estimation process is usually referred to as *Simultaneous Localization and Mapping* (SLAM). While the maturity of SLAM in both single robot and multi robot scenarios has been recognized by the robotic community, see [12], [13], the problem of planning under uncertainty with application to robotic exploration still remains an open issue. The corresponding problem is usually referred to as *active SLAM and exploration*. The goal of the active strategies addressing this problem is the accomplishment of a suitable trade-off between maximizing the mapped area and guaranteeing localization accuracy. While the importance of the exploration task is quite intuitive, the need of imposing suitable constraints on the admissible uncertainty stems from two different reasons: on one hand, such constraints can be due to mission requirements (e.g., high uncertainty in the map model can be undesirable in a rescue task if human intervention is planned on the basis of such world model); on the other hand, *the need of imposing bounds on the admissible uncertainty stems from reasons that are intrinsic to the estimation process*. In the following we will try to shed some light on the previous sentence. In Extended Kalman Filter (EKF) SLAM and variants (Sparse Extended Information Filter SLAM, Delayed State EKF-SLAM, etc.) the main hypothesis consists in assuming the posterior to be normally distributed. In order to preserve the Gaussianity of the posterior, the nonlinear models describing robot motion and the available measurements need to be linearized. However, the linear approximation is effective only if the first-order approximation properly describes the behavior of the nonlinear system in a neighborhood of the linearization point, and the dimension of such a neighborhood is connected with the amount of uncertainty in the posterior [26]. As a consequence, for large amount of uncertainty, the linear approximation may not correctly model the problem and the effect of such phenomenon is that the actual probability density describing the SLAM posterior can no longer be approximated with a Gaussian density. This is not a mere approximation issue: if the posterior description is not consistent with the actual estimation errors, the filter is likely to diverge leading to the failure of the exploration (and mapping) task [8], [9].

A second widespread category of approaches to SLAM is based on Rao-Blackwellized Particle filters. In this paradigm, the Rao-Blackwell factorization is applied for decoupling the localization and the mapping problem, and the pose estimation is entrusted to a particle filter, see [11], [26]. The assumption underneath the RBPF algorithm is that the posterior density can be properly approximated by a point-mass (particles) representation. By increasing the number of the samples, it is possible to obtain better approximations of the posteriors [10]. However, since the complexity of the approach grows with the particle set size, normal processors can only handle few hundreds particles. A limited number of particles can be not adequate for assuring a proper approximation of the trajectory posterior and this issue becomes critical when the uncertainty in the posterior increases [15]. Because of the factorization, a bad approximation of the trajectory posterior affects the estimated map quality, hence, a constraint on the uncertainty of the trajectory posterior is desirable for accomplishing consistent mapping.

At this point, it should be clear that the active SLAM task requires suitable metrics for evaluating the uncertainty, so that the corresponding uncertainty bounds can be assessed. In EKF-like techniques such metric can be easily inferred from the covariance matrix describing the multivariate posterior (e.g., determinant, trace, entropy) [4], [16], [21]. On the other hand, for particle filter-based representation, it is not straightforward to quantify the uncertainty and to understand how it affects the result of the mapping process [3], [22].

In this paper we extend the results of our previous work [5], proposing an extensive evaluation of state-of-the-art approaches to active SLAM and exploration with particle filters, applied to the estimation of occupancy grid map representations of an indoor environment [18]. Such evaluation is challenging because of the lack of effective benchmark scenarios for active SLAM and exploration and suitable metrics for comparing the effectiveness of a technique. The paper is organized as follows. Section II reviews the basics of RBPF-SLAM, whereas in Section III we illustrate in details

This work was partially funded by Ministero dell'Istruzione, dell'Università e della Ricerca under MEMONET National Research Project, and by Regione Piemonte under MACP4log Grant (RU/02/26).

J. Du, B. Bona and M. Indri are with Dipartimento di Automatica e Informatica, Politecnico di Torino, Torino, Italy, {jingjing.du, basilio.bona, marina.indri}@polito.it

L. Carlone and M. Kaouk Ng are with CSPP, Laboratorio di Meccatronica, Politecnico di Torino, Torino, Italy, {luca.carlone, miguel.kaoukng}@polito.it

three active SLAM and exploration algorithms, namely the *joint entropy* [22], the *expected map information gain* [2], [3], and *the expected information from a policy* [5]. The comparative study and the experimental results are presented in Section IV, while final conclusions and future perspectives are discussed in Section V.

II. Rao-Blackwellized Particle Filters SLAM

Although the high dimensionality of state space in grid-based SLAM makes challenging the application of sample-based representations of the posterior of robot pose and occupancy grid map, an elegant solution to reduce dimensionality of the sampling space can be obtained through Rao-Blackwellization [11]. Since the map probability can be computed analytically given the robot path, it is possible to factorize the joint probability as follows:

$$p(\mathbf{x}_{1:t}, m \mid \mathbf{z}_{1:t}, \mathbf{u}_{0:t-1}) = p(m \mid \mathbf{x}_{1:t}, \mathbf{z}_{1:t}) \cdot p(\mathbf{x}_{1:t} \mid \mathbf{z}_{1:t}, \mathbf{u}_{0:t-1}) \quad (1)$$

In (1) the state includes the robot trajectory $\mathbf{x}_{1:t} = \{\mathbf{x}_1, \mathbf{x}_2, \ldots, \mathbf{x}_t\}$ and the map m, both estimated from the measurements $\mathbf{z}_{1:t} = \{\mathbf{z}_1, \mathbf{z}_2, \ldots, \mathbf{z}_t\}$ and the commands $\mathbf{u}_{0:t-1} = \{\mathbf{u}_0, \mathbf{u}_1, \ldots, \mathbf{u}_{t-1}\}$. Equation (1) provides the basis for RBPF-SLAM: the particle filter is applied to the problem of estimating potential trajectories and a map hypothesis is associated to each sample. According to particle filter framework the posterior of robot trajectory is approximated by a set of weighted random samples:

$$p(\mathbf{x}_{1:t} \mid \mathbf{z}_{1:t}, \mathbf{u}_{0:t-1}) \approx \sum_{k=1}^{n} \omega_t^{[k]} \delta(\mathbf{x}_{1:t} - \mathbf{x}_{1:t}^{[k]}) \quad (2)$$

where n is the particle set size, $\mathbf{x}_{1:t}^{[k]}$ is the pose of the k-th particle at time t, $\omega_t^{[k]}$ is the corresponding weight $\left(\sum_{k=1}^{n} \omega_t^{[k]} = 1\right)$, and $\delta(\cdot)$ is the Dirac delta function. Filter prediction is obtained by drawing particles from the *proposal distribution* $\eta(\mathbf{x}_{t+1} \mid \mathbf{x}_t, \mathbf{u}_t)$, which is often approximated with a Gaussian density, whose mean and covariance depend on the odometric information $\mathbf{u}_t$, whereas the weights are updated according to [23]:

$$\omega_t^{[k]} = \omega_{t-1}^{[k]} p(\mathbf{z}_t \mid \mathbf{x}_{t-1}^{[k]}, \mathbf{u}_{t-1}, m_{t-1}^{[k]}), \quad k = 1, \ldots, n \quad (3)$$

Particles degeneracy (i.e., the situation in which most part of the sample set has negligible weight) is then prevented by a resampling phase that randomly chooses the samples that best fit current and past observations, according to particles weights. A common condition for resampling is based on the *effective sample size* [1], which is an approximated measure of particle diversity:

$$\tilde{N}_{eff} = \frac{1}{\sum_{i=1}^{n} \left(\omega_t^{[k]}\right)^2} \quad (4)$$

Particles are re-sampled if the previous quantity drops below a given threshold, usually fixed to $n/2$, see [24].

Since normal processors can only carry out estimation with few hundred samples, when the uncertainty in robot localization increases (e.g., the robot is traversing a long trajectory in open loop, without revisiting known places), the particle-based belief approximation degrades and loop-closing occurrence becomes crucial. A degradation of particle-based approximation influences the quality of the estimated map, hence an active policy is required: performing simple exploration (i.e., choosing the motion targets so to maximize the amount of explored areas) may lead to inconsistent map model, making the exploration process inefficient.

III. Active SLAM and Exploration with RBPF

It is possible to interpret active SLAM and exploration as an optimization problem: given the information acquired until the current time (included in the SLAM posterior), the robot has to choose an exploration target (i.e., a goal point to be reached) so that the corresponding *information gain* is maximized. All the techniques for active SLAM and exploration with particle filters cannot compute a global optimum, i.e., they cannot estimate the best target over the whole map, because of the lack of closed-form expressions for the information gain. Therefore, state-of-the-art approaches make use of simulation for evaluating the information gain in few possible target points (lately referred to as *target candidates*). A widespread strategy for selecting such target candidates will be presented in Section III-A, with application to occupancy grid map representations. A formal definition of *information gain*, instead, will be presented in Section III-B, since each compared technique is characterized by a different metric for evaluating such gain.

A. Target Selection

In this section we briefly recall the *frontier-based exploration* approach for target selection, proposed in [27], [28]. A *frontier* cell is on the boundary between visited and unexplored areas. Using occupancy grid map representation [18], unvisited areas are modeled with cells having occupation probability of 0.5, whereas visited cells assumes values close to 1 (respectively 0) if they contain obstacles (respectively free space). It is clear that the boundary between an area containing cells with values smaller than 0.5 and an area with cells having value equal to the prior probability 0.5 offers the robot a possibility of visiting new places, hence they are desirable target candidates. Moreover, when no frontier does exist in the map, the exploration process can be considered concluded and no target needs to be reached.

As pointed out in [27], the frontier detection can be carried on with simple techniques that resemble the edge detection process in computer vision. Moreover, for reducing the effects of false frontiers (due for instance to outliers in sensor readings), it is possible to cluster the frontier cells and to associate target candidates to clusters with size comparable to robot dimensions. In addition to the approach proposed in [27], we also add some candidate targets along the trajectory traveled by the robot: this second set of candidates allow the robot to come back to known places when filter uncertainty is high. It is worth remarking that it is desirable to express the target positions in the reference frame of the robot since in this way it is no longer needed to have a list of candidate targets for each sample in the filter.

B. State-of-the-art approaches

In this section we present three techniques for solving the active SLAM and exploration problem. Before entering in the details of each technique we mention that such approaches are finalized to evaluate the information gain in reaching a given target candidate; therefore the target candidate for which the expected gain is maximum, will be selected as a goal for robot motion. After reaching the *exploration goal* (or *goal target*), the decisional process will be iterated until the target selection phase (Section III-A) will produce no candidate target. It is worth noticing that naive criteria for selecting the exploration goal among the target candidates do exist; for instance in [27] the nearest target candidate

is selected as goal target. Another straightforward metric for goal selection is based on the number of cells that the robot is expected to visit when reaching such target, i.e., the goal point is the target for which the number of visited cells is maximized (a cell is considered to be visited if the corresponding probability is different from 0.5, see the previous section). It is clear that the naive approaches only address the exploration problem, since the probabilistic nature of the estimation process is completely neglected. More complex techniques that we are going to discuss in this section were proposed to cope with such aspects of active SLAM and exploration.

1) Joint Entropy: This technique is based on the joint entropy of path and trajectory posterior. The information gain at a target is evaluated using the entropy of both the robot trajectory and the map carried on by each particle, weighted by each trajectory's importance weight [22]. The *joint entropy* of robot position and map in RBPF is:

$$H\left(p(\mathbf{x}_{1:t}, m \mid \mathbf{d}_{1:t})\right) \approx H\left(p(\mathbf{x}_{1:t} \mid \mathbf{d}_{1:t})\right) + + \sum_{k=1}^{n} w_t^{[k]} H\left(p(m^{[k]} \mid \mathbf{x}_{1:t}^{[k]}, \mathbf{d}_{1:t})\right) \quad (5)$$

where n is the number of particles in the filter, $w_t^{[k]}$ is the weight of the *k*-th particle at time step t, $\mathbf{x}_{1:t}^{[k]}$ and $m^{[k]}$ are the trajectory and the map associated with the *k*-th particle respectively, the data $\mathbf{d}_{1:t} = \{\mathbf{z}_{1:t}, \mathbf{u}_{0:t-1}\}$ comprise both exteroceptive measurements and odometry. The first summand in (5) quantifies path entropy, whereas the second one corresponds to the entropy of the map estimation process. The entropy of the k-th map in the filter can be easily computed as:

$$H\left(p(m^{[k]} \mid \mathbf{x}_{1:t}^{[k]}, \mathbf{d}_{1:t})\right) = \sum_{\forall i,j} H(p(m_{ij}^{[k]} \mid \mathbf{x}_{1:t}^{[k]}, \mathbf{d}_{1:t})) \quad (6)$$

where $p(m_{ij}^{[k]} \mid \mathbf{x}_{1:t}^{[k]}, \mathbf{d}_{1:t}))$ describes the probability of a single cell in the occupancy grid map (corresponding to the indexes i and j) and the binary entropy function $H(\cdot)$ satisfies $H(p) = -p\log(p) - (1-p)\log(1-p)$.

For the computation of trajectory posterior entropy, in [20] it has been proposed to approximate the entropy of the point mass distribution with the entropy of the Gaussian distribution fitting particle poses, as follows:

$$H\left(p(\mathbf{x}_{1:t} \mid \mathbf{d}_{1:t})\right) \approx \frac{1}{t} \sum_{\tau=1}^{t} H\left(p(\mathbf{x}_{\tau} \mid \mathbf{d}_{1:\tau})\right) \quad (7)$$

where $p(\mathbf{x}_{\tau} \mid \mathbf{d}_{1:\tau})$ is a Gaussian approximation of pose posterior at time τ.

Therefore, the best exploration target is selected so to maximize the joint entropy reduction (i.e., smaller entropy at a target corresponds to higher information gain):

$$G_{\mathrm{H}} = H\left(p(\mathbf{x}_{1:t}, m \mid \mathbf{d}_{1:t})\right) + - H\left(p(\mathbf{x}_{1:t+T(\pi)}, m \mid \mathbf{d}_{1:t+T(\pi)})\right) \quad (8)$$

where current and predicted joint entropies are computed at time t and $t + T(\pi)$, and $T(\pi)$ is the time required for executing the motion policy π.

Although joint entropy is a widespread approach for particle-filter based exploration, some drawbacks are commonly recognized:

1) it depends on the overall grid area, instead of the actual observed cells;
2) it depends on the grid resolution, which is the reason why the entropy of any map increases unbounded when the resolution increases. This consideration and the previous one suggest the impossibility of fixing an absolute threshold as condition for active loop-closing;
3) if the robot entropy is computed using Gaussian fitting as in [20], [25], the method leads to the entropy divergence when only one particle survives from resampling (common after loop closing) unless ad-hoc heuristics are applied;
4) path entropy contribution is negligible with respect to map entropy, which has commanding influence on H.

The computational complexity of joint entropy is $O(n(M + l))$, where M is the number of cells in the map and l is the length of trajectory for reaching the target. The objective function F_{H}, the target has to maximize, includes some cost criterion to penalize far targets [4], [25]:

$$F_{\mathrm{H}} = G_{\mathrm{H}} - \alpha l \quad (9)$$

where α is a suitable weight for the path length l.

2) Expected Map Mean Information: In order to avoid some of the undesirable properties of joint entropy, the *expected map mean information* has been proposed in [2], [3]. Before introducing this information metric, the concept of *Expected Map (EM)* for RBPF needs to be briefly reviewed. Taking into account all the maps associated to the samples in the filter, *EM* is defined as the mathematical expectation $E[\,\cdot\,]$ of the map hypotheses over the particle set:

$$p(EM \mid \mathbf{d}_{1:t}) = E_{\mathbf{x}_{1:t}}\left[p(m \mid \mathbf{x}_{1:t}, \mathbf{d}_{1:t})\right] \quad (10)$$

Each cell i, j of the expected map can be obtained as:

$$p(EM_{ij} \mid \mathbf{d}_{1:t}) \approx \sum_{k=1}^{n} w_t^{[k]} p(m_{ij}^{[k]} \mid \mathbf{x}_{1:t}^{[j]}, \mathbf{d}_{1:t}) \quad (11)$$

The information is hence computed on the expected map:

$$I\left(p(EM \mid \mathbf{d}_{1:t})\right) = \sum_{\forall i,j} I(p(EM_{ij} \mid \mathbf{d}_{1:t})) \quad I\left(p(EM_{ij} \mid \mathbf{d}_{1:t})\right) = 1 - H(p(EM_{ij} \mid \mathbf{d}_{1:t})), \quad (12)$$

where $H\left(p(EM_{ij} \mid \mathbf{d}_{1:t})\right)$ is the entropy of a grid cell in the expected map.

As a consequence, the information gain after the execution of the motion action π can be defined as:

$$G_{\mathrm{EMMI}} = I\left(p(EM \mid \mathbf{d}_{1:t+T(\pi)})\right) - I\left(p(EM \mid d_{1:t})\right) \quad (13)$$

The expected map information (EMMI) can be applied to the problem of detecting an already traversed loop, nevertheless the computation of the gain is involving in terms of computation and memory requirements [3]. Since the expected map depends on the particles weights, and cannot be incrementally updated, its complexity is $O(nM)$. Moreover it is not clear how to fix a threshold on EMMI in order to assure consistent mapping (i.e., an absolute condition for loop closing). As for the joint entropy, the objective function for exploration is augmented with a term penalizing long paths:

$$F_{\mathrm{EMMI}} = G_{\mathrm{EMMI}} - \alpha l \quad (14)$$

where α is a suitable weight for the path length l.

3) Expected Information from a Policy: In our previous work [5] we proposed the use of the Kullback-Leibler divergence to evaluate the particle-based SLAM posterior approximation. In fact, all the previous techniques are based on the assumption that the particle filter correctly models SLAM posterior, whereas we already pointed out that a metric for evaluating filter approximation is desirable for reliable mapping. Such metric can be easily included in the definition of the information gain as discussed hereafter. Applying the Kullback-Leibler divergence it is possible to derive an upper bound on the divergence $\bar{\xi}$ between the true posterior $p(\mathbf{x}_t \mid \mathbf{d}_{1:t})$ and the approximated pose belief $\hat{p}(\mathbf{x}_t \mid \mathbf{d}_{1:t})$ at time t,

$$\xi(\hat{p}(\mathbf{x}_t \mid \mathbf{d}_{1:t}), p(\mathbf{x}_t \mid \mathbf{d}_{1:t})) < \bar{\xi},$$
$$\bar{\xi} = \frac{k_t - 1}{2n}\left[1 - \frac{2}{9(k_t-1)} + \sqrt{\frac{2}{9(k_t-1)}}\zeta_{1-\delta_t}\right]^3, \quad (15)$$

where n is the particle set size, k_t is the number of bins in which at least one particle falls, and $\zeta_{1-\delta_t}$ is the upper $1-\delta_t$ quantile of the standard normal distribution.

According to (15), for each pose $x_\tau, \tau = 1, 2, ..., t$ we can define an upper bound $\bar{\xi}_\tau$ on the approximation error with a given probability $1-\bar{\delta}$. Let the error of approximation of trajectory posterior be defined as:

$$\xi(p(\mathbf{x}_{1:t}, \mathbf{d}_{1:t})) = \xi(p(\mathbf{x}_t^*, \mathbf{d}_{1:t})), \quad (16)$$
$$\mathbf{x}_t^* = \underset{\tau \in [1:t], \delta_\tau = \delta}{\arg\max} (\bar{\xi}_\tau)$$

that is we assign to $\xi(p(\mathbf{x}_{1:t}, \mathbf{d}_{1:t}))$ the error of the pose which is expected to provide the worst approximation. Equation (16) formalizes the observation that the trajectory estimation, thus the map quality, can be compromised if also a single pose is affected by large errors.

According to equation (16), and since $\bar{\xi}_\tau$ is monotonically increasing in the number of non-empty bins, we can derive the probability of having a trajectory error less than $\bar{\xi}$ as:

$$p(\xi(p(\mathbf{x}_{1:t}, \mathbf{d}_{1:t})) < \bar{\xi}) = p(\xi(p(\mathbf{x}_t^*, \mathbf{d}_{1:t})) < \bar{\xi}) = \quad (17)$$
$$= \mathcal{F}\left\{\left[\sqrt{\frac{9(k^*-1)}{2}} - \left(\sqrt[3]{\frac{2n\bar{\xi}}{k^*-1}} + \frac{2}{9(k^*-1)} - 1\right)\right]\right\},$$

where $k^* = \max\{k_\tau, i \in [1:t]\}$ and $\mathcal{F}(\cdot)$ is the cumulative distribution function of a standard Gaussian distribution.

Under the assumption that the sample size n is fixed, this probability is influenced by two parameters: the number of non-empty grids, and the error bound $\bar{\xi}$. In our previous papers [5], [6], we detailed how to choose proper parameters so that $p(\xi(p(\mathbf{x}_{1:t}, \mathbf{d}_{1:t})) < \bar{\xi})$ actually reflects the probability of the mapping process to be successful. Therefore, we can include such information as follows: after applying the motion policy π (towards a generic target candidate), with probability $p(t,\pi) = p(\xi(p(\mathbf{x}_{1:t}, \mathbf{d}_{1:t})) < \bar{\xi})$ the robot will totalize the information $I(m_{t+T(\pi)}) = I\left(p(m|\mathbf{x}_{1:t+T(\pi)}, \mathbf{d}_{1:t+T(\pi)})\right)$, or with probability $1-p(t,\pi)$ filter approximation will lead to map inconsistency, whose effect is the failure of the SLAM process, i.e., the amount of information after reaching the target will be zero. Taking the expectation over the two possible outcomes of the experiment we obtain the *expected information from the policy* π:

$$G_{\text{EI}} = p(t,\pi)[I(m_{t+T(\pi)}) - I(m_t)] + \\ +(1-p(t,\pi))[-I(m_t)] \quad (18)$$

where $p(t,\pi) = p(\xi(p(\mathbf{x}_{1:t+T(\pi)}, \mathbf{d}_{1:t+T(\pi)}) < \bar{\xi})$ is the probability of map consistency. The concept of *expected information* allows not only to consider the information collected by the particle filter, but also to take into account the information loss due to the mapping inconsistency. Whenever the confidence of SLAM approximation is high ($p(t,\pi) \approx 1$), the robot will prefer to explore new areas since it attempts to obtain the maximum information $I(m_{t+T(\pi)})$. However, if particle approximation degrades, robot will prefer moving to known places, so to increase the value of $p(t,\pi)$.

Notice that we did not explicit the definition of the information $I(m_t)$, hence also the metrics presented in Section III-B.1 and III-B.2 may be considered. In this context, to overcome the computation effort that characterizes related work, we simplify the map information considering only the number of observed free grid cells N_t, hence $I(m_t) = N_t$. Equation (18) can be then simplified to:

$$G_{\text{EI}} = p(t,\pi)N_{t+T(\pi)} - N_t \quad (19)$$

In order to consider the cost of traveling the distance to the target we proposed the use of a *specific information gain from the policy*:

$$F_{EI} = \frac{G_{\text{EI}}}{l} \quad (20)$$

in which the actual information is normalized by the traveled distance. Therefore the specific information assumes the meaning of a gain for each traveled meter, and intrinsically takes into account the disadvantage of reaching targets which are far away. We preferred not to use the additive cost functions like (9) and (14) so to avoid the introduction of parameter α that has to be set experimentally and can be scenario-dependant.

IV. Experimental Results

For the purpose of evaluating the techniques presented so far in realistic scenarios, we have carried out extensive tests in typical indoor environments, simulating the case in which a robot, equipped with a laser range finder is deployed in the scenario and is required to explore it, producing a consistent representation in the form of an occupancy grid map. The range of the laser-scanner is 16 m, whereas the number of particles in the filter was set to 50. Instead of considering manually designed simulation scenarios that can be an oversimplification of real exploration procedures and that may be not able to catch the complexity of a real environment, we started from real maps and converted them in the corresponding representation to be use in the MobileSim simulator [17]. We preferred to use maps that are well-known to the robotic community so to make the experiments clearer, and for sake of repeatability we will release an online version of all the employed maps at [19]. In particular we considered three test scenarios: 1) the ACES building at the University of Texas, which covers an area of about 45 m by 40 m (Figure 1(a)); 2) the map recorded at the Intel Research Lab in Seattle with the size of 28 m by 28 m (Figure 1(b)) and 3) University of Freiburg 079 building, in which the main corridor length is about 36 m (Figure 1(c)). Without entering in the details, we specify that the aforementioned maps were available online as occupancy grid maps (see [14] for instance) but needed to be converted in a proper format to be used in MobileSim; Figures 1(a)-(c) contain the already processed maps.

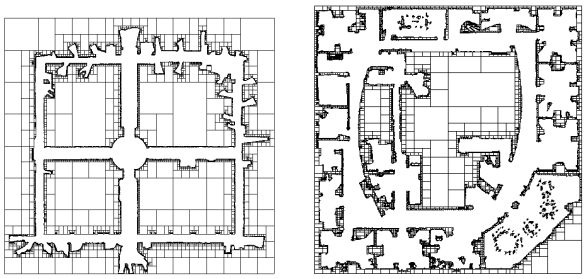

(a) ACES (b) Intel

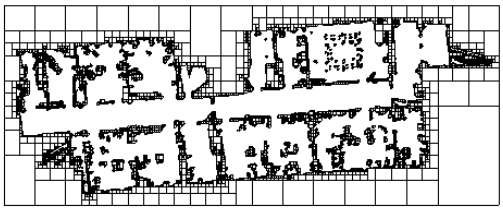

(c) Freiburg 079 building

Fig. 1. (a) MobileSim map of the ACES building; (b) MobileSim map of the Intel Research Lab; (c) MobileSim map of the Freiburg 079 building.

A. Case studies

First of all we consider three case studies to remark the peculiarity of the aforementioned approaches. In order to evaluate the influence of path length cost parameter α in Joint entropy F_H and Expected map mean information F_{EMMI} (see equations (4) and (9)), we tested the performance of these approaches for different values of α. We also report the length of the path required to reach each candidate target and a naive metric (N) to help the comparison with the other approaches; the naive metric N evaluates the expected number of cells to be visited (i.e., cells with probability of occupation different from 0.5) when reaching a target. For each candidate target we report the following values:

1) Expected information from a policy (F_{EI});
2) Joint entropy (F_H) with $\alpha = 100$;
3) Joint entropy (F_H) with $\alpha = 200$;
4) Expected map mean information (F_{EMMI}), $\alpha = 100$;
5) Expected map mean information (F_{EMMI}), $\alpha = 200$;
6) Naive metric (N);
7) Path length to reach each candidate target.

The following case studies were selected during the tests on the ACES building (Figure 1(a)); this scenario is particularly relevant for our analysis because the presence of crossroads allows to clearly discern the differences in the decisional processes that lie behind each exploration approach.

1) Case 1: in Figure 2(a) the robot starts to explore the environment and reaches the point labeled with a red circle. At this point it performs target selection, according to the frontier-based technique presented in Section III-A, and obtains the target candidates that are plotted in the figure as blue circles. This case study is important because the environment offers the robot the opportunity to perform a loop closing, reducing the SLAM posterior uncertainty and we are now interested in evaluating the score assigned by the different approaches to each target.

Let us start our discussion from the joint entropy. In Figure 2(e) the cost of traversing long distances has smaller weight ($\alpha = 100$) and the information content of the target is dominant in the definition of the goal target: in this case, as we anticipated in [5], F_H is not able to catch the loop closing opportunity and prefers selecting targets that maximize the possibility of visiting new cells. Comparing this figure with Figure 2(d) it is clear that the behavior of F_H ($\alpha = 100$) is the same as the naive metric, although the evaluation of the number of observed cells (N) is less demanding than the computation of the joint entropy. It is clear from the same figure that this metric completely misses the *active SLAM* aspects of the problem at hand: F_H is not able to measure filter uncertainty and for this reason the metric suggests the robots only to solve the *exploration* problem. In Figure 2(f) we report the case of F_H ($\alpha = 200$), in which the cost associated with the distance from the target is crucial in the goal selection. In this case the outcome suggests that the behavior of the joint entropy can be directly deduced by the path length, see Figure 2(b): the scores are high for short paths and low for long paths, hence reducing the exploration approach to the choice of the nearest target candidate. When using the Expected Map Mean Information, see Figures 2(g)-(h), the scores of the targets resembles the corresponding scores in F_H. Few differences appear, in particular between Figure 2(e) and Figure 2(g), since the target candidate #3 acquires a higher score; however such a difference does not improve the exploration effectiveness: target #3 does not correspond to a loop closing and both F_H and F_{EMMI} are only able to quantify the advantage in exploring an area, losing the probabilistic content of the problem and underestimating the risk of filter inconsistency. On the other hand, Figure 2(c) clearly remarks that the expected information from a policy (F_{EI}) is able to measure filter uncertainty and returns a high score for target #6 which corresponds to a loop closing. It is worth noticing that, because of the size of the environment, if the robot misses this loop closing and continues on the corridor towards target #3 the uncertainty in the posterior will unavoidably lead to a failure of the mapping process.

2) Case 2: in Figure 3(a) the robot has already completed a first loop closing and reaches a second crossroad in which it has to decide between exploring new areas (i.e., going straight on towards target #1) or closing the loop (turning towards target #5). Also this case study remarks the previous observation on the state-of-the-art approaches: F_H ($\alpha = 200$) and F_{EMMI} ($\alpha = 200$) resembles the inverse behavior of the path length, i.e., the distance from the path is crucial in the determination of the goal target; F_H ($\alpha = 100$) and F_{EMMI} ($\alpha = 100$) present few differences with respect to N, hence questioning the need of using complex metrics for planning. The expected information from a policy F_{EI}, however, is able to provide a different answer to the target scoring problem, and such metric, though being influenced by the path length and by N, provides a balanced mix of both aspects, preserving the probabilistic description of the problem.

3) Case 3: similar considerations hold for the last case study reported in Figure 4. In this situation it is even more evident that F_{EI} is able to provide an effective strategy for active SLAM and exploration, underlining the importance of targets corresponding to loop closings (e.g., targets #500 and #501); other approaches, instead, assign low scores to these targets, see Figures 4(e)-(h).

In Table I we summarize the results of the three case studies by reporting only the best target (i.e., the target that will be selected as goal for robot motion) depending on the exploration approach. It should be clear that, for F_H and F_{EMMI}, the cost associated with the path length is hard to balance and the parameter α is only able to trade-off

TABLE I

GOAL TARGET SELECTED BY EACH OF THE COMPARED APPROACHES FOR THE THREE CASE STUDIES UNDER ANALYSIS.

Case studies	F_{EI}	F_H		F_{EMMI}		N
		$\alpha = 100$	$\alpha = 200$	$\alpha = 100$	$\alpha = 200$	
1	6	9	6	9	3	9
2	5	11	5	11	5	11
3	501	2	7	9	7	9

between two suboptimal strategies, i.e., (i) maximizing the number of visited cells and (ii) moving towards the nearest target candidate. On the other hand F_{EI} is able to model filter uncertainty and allows to evaluate the risk of map inconsistency when performing an action.

B. Autonomous Exploration experiments

After providing some insights on the decisional process that lies behind the compared techniques we want to apply them in autonomous exploration experiments, evaluating the potential of the strategies in solving real navigation problems. Therefore, the robot is deployed in an arbitrary position in one of the three scenarios (Figure 1) and the test is repeated three times for each approach, for a total of 45 experiments. The exploration procedures are compared in terms of time required for exploration, average quality of the estimated map and robustness.

Firstly we need to introduce a metric for evaluating the goodness of the mapping process. Since we have a *ground truth* map on which the simulation scenario is built, we simply need to introduce a measure of similarity between the true map and the map estimated with the different exploration approaches. This measure of map similarity is provided in the following definition.

Definition: Let M_1 and M_2 be two grid maps. The agreement between M_1 and M_2 (indicated as $\text{agr}(M_1, M_2)$) is the number of cells in M_1 and M_2 that are both free or both occupied. The disagreement between M_1 and M_2 (indicated as $\text{dis}(M_1, M_2)$) is the number of cells such that M_1 is free and M_2 is occupied or vice-versa, moreover the disagreement also includes the number of cells that are unvisited in M_1 and turn out to be observed in M_2. The *acceptance index* $\omega(M_1, M_2)$ between the maps is defined as:

$$\omega(M_1, M_2) = \frac{\text{agr}(M_1, M_2)}{\text{agr}(M_1, M_2) + \text{dis}(M_1, M_2)}. \quad (21)$$

The acceptance index, ranging between 0 and 1, measures map similarity, once a suitable roto-translation is applied.

It is worth noticing that the *acceptance index* was introduced in [7], but Carpin's definition does not consider the unvisited cells in the evaluation of the disagreement: assuming M_1 to be the true map, it is evident that the estimated map cannot contain more information than the original one, hence we preferred to include in the disagreement the fact that cells that are unknown in the true map, cannot have a probability different from the prior 0.5 in the estimated map. Examples of acceptance indexes for maps estimated in our tests are reported in Figure 5.

In Table II we report the acceptance indexes for the different approaches in the tested scenarios. We remark that the acceptance index in the table indicates the average quality of the map estimated with a given approach, the exploration time is connected with the computational complexity of the approach, whereas the number of failure can be considered as an indicator of the robustness of the approach.

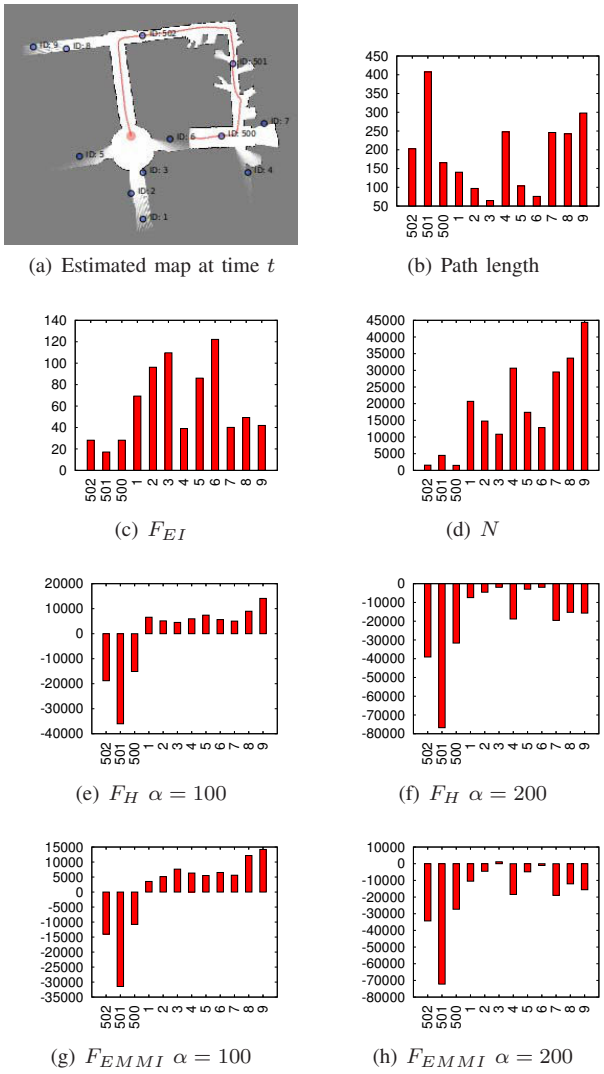

(a) Estimated map at time t (b) Path length

(c) F_{EI} (d) N

(e) F_H $\alpha = 100$ (f) F_H $\alpha = 200$

(g) F_{EMMI} $\alpha = 100$ (h) F_{EMMI} $\alpha = 200$

Fig. 2. Case study 1: (a) map of the scenario including robot position (red circle) and the position of the candidate targets (blue circles), where candidate targets from #1 to #9 are located in the frontier areas and candidate targets from #500 to #502 lie on the trajectories traveled by the robot; (b) path length for each candidate targets; (c)-(h) bar plot of the scores for each target in (a) according to the compared metrics.

Let us start our discussion considering the results of autonomous exploration at the Freiburg 079 building. The scenario comprises a main corridor and several small offices. This structure suggests that the robot is forced to traverse several times the corridor, hence, forcing several loop closings. For this reason we expect all the techniques to have good performance, also because of the small size of the environment. This expectation is confirmed by the acceptance index of the different approaches in Table II. Map quality is quite high in all the cases and failures in the mapping process are rare. It is possible to notice that the average time required by the F_{EI} is smaller than the compared approaches and the use of a small α in F_H and F_{EMMI} leads to an increase in the exploration time, since the robot often moves towards far targets, neglecting the cost associated with the distance traveled and the accumulation of uncertainty when traversing large areas in open loop. Similar

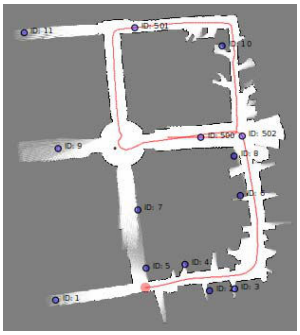

(a) Case study 2

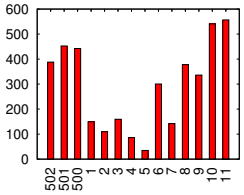

(b) Path length

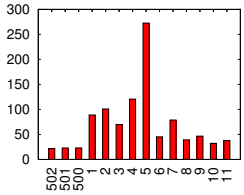

(c) F_{EI}

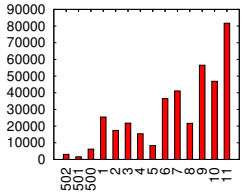

(d) N

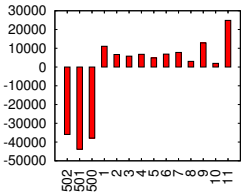

(e) F_H $\alpha = 100$

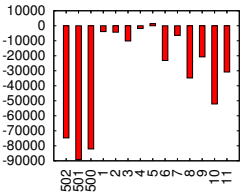

(f) F_H $\alpha = 200$

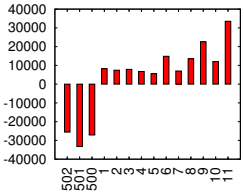

(g) F_{EMMI} $\alpha = 100$

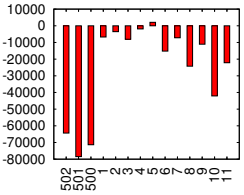

(h) F_{EMMI} $\alpha = 200$

Fig. 3. Case study 2: (a) map of the scenario including robot position (red circle) and the position of the candidate targets (blue circles), where candidate targets from #1 to #11 are located in the frontier areas and candidate targets target from #500 to #502 lie on the trajectories traveled by the robot; (b) path length for each candidate targets; (c)-(h) bar plot of the scores for each target in (a) according to the compared metrics.

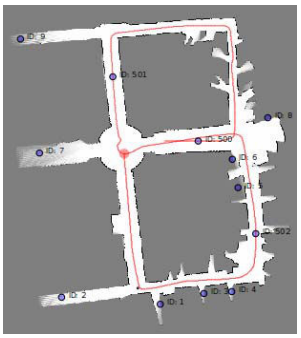

(a) Case study 3

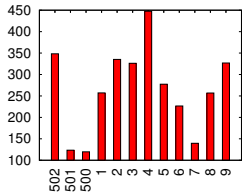

(b) Path length

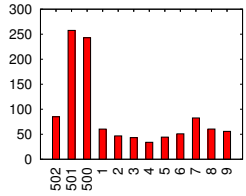

(c) F_{EI}

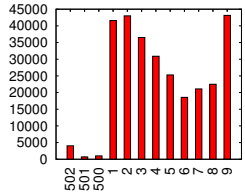

(d) N

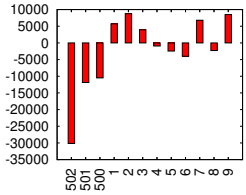

(e) F_H $\alpha = 100$

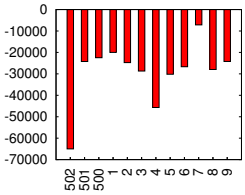

(f) F_H $\alpha = 200$

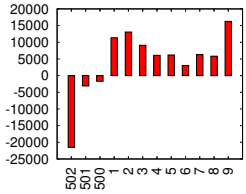

(g) F_{EMMI} $\alpha = 100$

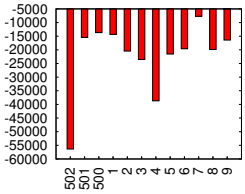

(h) F_{EMMI} $\alpha = 200$

Fig. 4. Case study 3: (a) map of the scenario including robot position (red circle) and the position of the candidate targets (blue circles), where candidate targets from #1 to #9 are located in the frontier areas and candidate targets from #500 to #502 lie on the trajectories traveled by the robot; (b) path length for each candidate targets; (c)-(h) bar plot of the scores for each target in (a) according to the compared metrics.

observations can be done with regard to the Intel research lab. In the corresponding rows of Table II we notice that there is a small difference between the average map quality. However in this case, the number of failures starts to be relevant for the presence of several areas to be explored and several obstacles that remark the role of a proper motion strategy. The exploration time for the expected information from a policy F_{EI} is higher than most of the other techniques, but this surplus of time is justified by a higher robustness in the mapping process. The other techniques, although being acceptable on the average acceptance index, often incur in map inconsistency.

The most challenging test bench is the ACES building, and robot decision making is crucial in accomplishing a consistent map estimation. In the previous scenarios, the size and the structure of the environment forces the robot to revisit

(a)

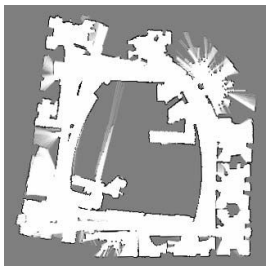

(b)

Fig. 5. (a) Example of consistent map with acceptance index $\omega = 0.84$; (b) Example of inconsistent map with acceptance index $\omega = 0.74$. Both acceptance indexes are computed with respect to the ground truth map.

TABLE II

AUTONOMOUS EXPLORATION PERFORMANCES WITH STATE-OF-THE-ART APPROACHES. ACCEPTANCE INDEXES, TIME REQUIRED FOR COMPLETING THE EXPLORATION, AND NUMBER OF FAILURES FOR EACH OF THE COMPARED APPROACHES.

		$\mathbf{F_{EI}}$	$\mathbf{F_H}$		$\mathbf{F_{EMMI}}$	
			$\alpha=100$	$\alpha=200$	$\alpha=100$	$\alpha=200$
FR079	$\omega(M_1, M_2)$	0.793	0.785	0.808	0.767	0.727
	Time (min)	102	157	95	149	116
	# Fail	0	0	0	0	1
Intel	$\omega(M_1, M_2)$	0.815	0.842	0.771	0.823	0.805
	Time (min)	212	138	199	242	174
	# Fail	0	0	2	0	2
ACES	$\omega(M_1, M_2)$	0.687	0.537	0.657	0.636	0.550
	Time (min)	226	331	250	369	330
	# Fail	2	3	3	3	3

known places, hence providing a natural reduction of the SLAM uncertainty. In this last case, instead, the presence of crossroads requires an effective exploration strategy: missing a loop closing means being unable to estimate a correct map, hence a wrong decision is clearly visible from the experimental results. The results show that in most cases all the techniques are likely to fail. The only approach which is able to produce meaningful results in one experiment is the F_{EI}. Clearly, the experiment can be made easier considering, for instance, a higher range for the laser, but we preferred to test a more challenging situation to have a clear picture of approach limitations.

V. CONCLUSION

This work investigates the problem of active SLAM and exploration with particle filters. We review the state-of-the-art on the topic and we recall the theoretical background of the mainstream approaches. Then we compare several techniques in realistic scenarios to evaluate the maturity of the field for solving real exploration problems that arise in rescue and coverage applications. Beyond the discussion of the peculiarities of the approaches that can be deduced from the mathematical definitions of the metrics used for establishing robot strategy, an interesting contribution of the paper stems from the experimental analysis. The exploration procedures are compared in terms of time required for exploration (hence, in terms of computational effort), average quality of the estimated map and robustness (i.e., number of failures in the mapping process). The test scenarios are well-known SLAM benchmarking environments and the map used in simulations will be available online [19] for stimulating future comparisons and discussions. The results provide an original insight on the exploration approaches, demonstrating that most of the mainstream approaches are not able to properly catch the probabilistic aspects of the problem and several state-of-the-art solutions present a cumbersome computational cost that is not justified by any performance improvement with respect to naive strategies (e.g., moving to the nearest exploration target). Future work consists in extending the presents results including more test scenarios and higher number of tests for increasing the statistical significance of the results.

VI. ACKNOWLEDGMENTS

Thanks to Niccolò Cascarano, Vito Macchia, Stefano Rosa and Federico Tibaldi for their support in the test campaign.

REFERENCES

[1] S. Arulampalam, S. Maskell, N. Gordon, and T. Clapp. A tutorial on particle filter for on-line nonlinear/non-gaussian bayesian tracking. *IEEE Trans. On Signal Processing*, 2(50):174–188, 2002.

[2] J. Blanco, J. Fernandez-Madrigal, and J. Gonzalez. An entropy-based measurement of certainty in Rao-Blackwellized particle filter mapping. In *Proc. of the IEEE-RSJ Int. Conf. on Intelligent Robotics and Systems*, pages 3550–3555, 2006.

[3] J. Blanco, J. Fernandez-Madrigal, and J. Gonzalez. A novel measure of uncertainty for mobile robot SLAM with Rao-Blackwellized particle filters. *Int. J. Robot. Res.*, 27(1):73–89, 2008.

[4] F. Bourgault, A. Makarenko, S. Williams, B. Grocholsky, and H. Durrant-Whyte. Information based adaptive robotic exploration. In *Proc. IEEE-RSJ Int. Conf. on Intelligent Robots and Systems*, 2002.

[5] L. Carlone, J. Du, M. Kaouk Ng, B. Bona, and M. Indri. An application of Kullback-Leibler divergence to active SLAM and exploration with particle filters. In *Proc. of the IEEE Int. Conf. on Intelligent Robots and Systems*, pages 287–293, 2010.

[6] L. Carlone, M. Kaouk Ng, J. Du, B. Bona, and M. Indri. Reverse KLD-sampling for measuring uncertainty in Rao-Blackwellized particle filters SLAM. In *Proc. of the IEEE-RSJ Int. Conf. on Intelligent Robots and Systems*, 2009.

[7] S. Carpin. Fast and accurate map merging for multi-robot systems. *Autonomous Robots*, 25:305–316, 2008.

[8] J. Castellanos, R. Martinez-Cantin, J. Tardós, and J. Neira. Robocentric map joining: Improving the consistency of EKF-SLAM. *Robotics and Autonomous Systems*, 55(1):21–29, 2007.

[9] J. Castellanos, J. Neira, and J. Tardós. Limits to the consistency of EKF-based SLAM. In *5th IFAC Symp. on Intelligent Autonomous Vehicles*, pages 1244–1249, 2004.

[10] D. Crisan and A. Doucet. A survey of convergence results on particle filtering methods for practitioners. *IEEE Transactions on signal processing*, 50(3):736–746, 2002.

[11] A. Doucet, N. de Freitas, K. Murphy, and S. Russel. Rao-Blackwellized particle filtering for dynamic bayesian networks. In *Proc. of the Conf. on Uncertainty in Artificial Intelligence*, pages 176–183, 2000.

[12] H. Durrant-Whyte and T. Bailey. Simultaneous localization and mapping (SLAM): Part I. *Robotics and Automation Magazine*, 13:99–110, 2006.

[13] H. Durrant-Whyte and T. Bailey. Simultaneous localization and mapping (SLAM): Part II. *Robotics and Automation Magazine*, 13:108–117, 2006.

[14] R. Kümmerle, B. Steder, C. Dornhege, M. Ruhnke, G. Grisetti, C. Stachniss, and A. Kleiner. Slam benchmarking webpage. *http://ais.informatik.uni-freiburg.de/slamevaluation*, 2009.

[15] R. Martinez-Cantin, N. de Freitas, and J. Castellanos. Analysis of particle methods for simultaneous robot localization and mapping and a new algorithm: Marginal-SLAM. In *Proc. of the IEEE lnternational Conf. on Robotics and Automation*, 2007.

[16] R. Martinez-Cantin, N. D. Freitas, A. Doucet, and J. Castellanos. Active policy learning for robot planning and exploration under uncertainty. In *Proc. of Robotics: Science and Systems*, 2007.

[17] MobileRobots Inc. Mobilesim, the mobile robots simulator. *http://robots.mobilerobots.com/MobileSim*.

[18] H. Moravec. Sensor fusion in certainty grids for mobile robots. *AI Magazine*, 9(2):61–74, 1988.

[19] Robotics Research Group (RRG). Politecnico di Torino. *www.polito.it/LabRob*.

[20] N. Roy, W. Burgard, D. Fox, and S. Thrun. Coastal navigation: Mobile robot navigation with uncertainty in dynamic environments. In *Proc. of Int. Conf. on Robotics and Automation*, pages 35–40, 1999.

[21] R. Sim and N. Roy. Global A-optimal robot exploration in SLAM. In *Proc. of the IEEE lnternational Conf. on Robotics and Automation*, pages 673–678, 2005.

[22] C. Stachniss, G. Grisetti, and W. Burgard. Information gain-based exploration using Rao-Blackwellized particle filters. In *Proc. of Robotics: Science and Systems*, 2005.

[23] C. Stachniss, G. Grisetti, and W. Burgard. Analyzing gaussian proposal distributions for mapping with rao-blackwellized particle filters. In *Proc. of Int. Conf. on Intelligent Robots and Systems*, 2007.

[24] C. Stachniss, G. Grisetti, D. Hahnel, and W. Burgard. Improved Rao-Blackwellized mapping by adaptive sampling and active loop-closure. In *Proc. of the Workshop on Self-Organization of AdaptiVE behavior*, pages 1–15, 2004.

[25] C. Stachniss, D. Hahnel, and W. Burgard. Exploration with active loop-closing for FastSLAM. In *Proc. of the IEEE-RSJ Int. Conf. on Intelligent Robots and Systems*, pages 1505–1510, 2004.

[26] S. Thrun, W. Burgard, and D. Fox. Probabilistic robotics. *MIT press*, 2005.

[27] B. Yamauchi. A frontier-based approach for autonomous exploration. In *Proc. of CIRA 97*, pages 146–151, 1997.

[28] B. Yamauchi. Frontier-based exploration using multiple robots. In *Proc. of the second Int. Conf. on Autonomous agents*, pages 47–53, 1998.